THE ASTROPHYSICAL JOURNAL, 365:321–331, 1990 December 10

X-RAY ILLUMINATED STELLAR WINDS: IONIZATION EFFECTS IN THE RADIATIVE DRIVING OF STELLAR WINDS IN MASSIVE X-RAY BINARY SYSTEMS

IAN R. STEVENS[1] AND TIMOTHY R. KALLMAN
Laboratory for High-Energy Astrophysics, NASA/GSFC, Greenbelt, Maryland
Received 1990 January 30; accepted 1990 June 8

ABSTRACT

The X-ray flux in massive X-ray binary systems is produced by the gravitational capture and accretion of material onto a neutron star from the wind of the early-type primary. The X-rays will in turn affect the dynamics of the stellar wind by changing the ionization and temperature structure in the wind and thus altering the radiative force experienced by the wind material. To further our knowledge of massive X-ray binary systems, it is necessary to study how the wind dynamics will be modified when the wind material is illuminated by a strong source of X-rays.

In this paper, the effect of X-ray ionization on the radiative force experienced by stellar wind material in a massive X-ray binary system is calculated. The radiative line force from the radiation field of the primary can be parameterized in terms of the Castor, Abbott, and Klein force multiplier $M(t)$. Results are presented for the variation of the line force multiplier $M(t)$ with the ionization parameter ξ (a measure of the degree of photoionization). These show that the line force decreases sharply with increasing X-ray ionization, though in a very nonlinear way. Some of the dynamical consequences of these results are briefly discussed, finding that the wind velocity can be severely decreased in the supersonic portion of the flow by X-ray ionization.

Subject headings: stars: winds — X-rays: binaries

I. INTRODUCTION

In massive X-ray binary systems (hereafter MXRBs) the primary star (an OB giant or supergiant) is losing mass via a dense supersonic stellar wind. In such systems, the secondary companion, usually a neutron star (though in Cyg X-1 a black hole secondary is considered more likely), is immersed in the stellar wind and accretes material from it, giving rise to a strong X-ray flux. In the case of early-type stars, the stellar wind is largely driven by the line absorption of radiation from the primary by the stellar wind material, and this mechanism can impart sufficient momentum to power large-scale mass loss (in some cases $\dot{M} \geq 10^{-6}\ M_{\odot}\ \mathrm{yr}^{-1}$) and drive the material to velocities of several thousand km s^{-1}. As shown by Abbott (1982), the momentum necessary to drive this mass flux comes from a very large assemblage of lines from a large number of atomic species.

The most successful model of stellar winds from early-type stars to date has been that of Castor, Abbott, and Klein (1975, hereafter CAK). CAK, building on work by Castor (1974), parameterized the radiative line acceleration from an early-type star in terms of a force multiplier $M(t)$ (eq. [7]). In the original CAK model, the force multiplier was calculated using only atomic data for the C III ion, the abundance of which was suitably scaled to mimic the total heavy ion abundance. A considerable improvement was made upon this by Abbott (1982) who compiled relatively complete atomic data for the first 30 elements in the periodic table (H to Zn), for typically the first six ionization stages. These calculations, when coupled with the improved stellar wind models of Pauldrach, Puls, and Kudritzki (1986), have led to significant improvements in the agreement between CAK type theory and the observations of the mass-loss rates and the terminal velocities of the winds of early-type stars. In addition, Puls (1987) has more recently presented results concerning the influence of multiline effects on the radiative line force multiplier.

These force multiplier results have been used by some authors (for example, Friend and Castor 1982; Stevens 1988) to calculate stellar wind models for binary systems. These models effectively ignored the modifications to the radiative line force that will result from X-ray ionization and concentrated on the gravitational influence of the neutron star companion on the wind of the early-type primary.

Previous attempts to model the dynamical consequences of X-ray photoionization on the wind dynamics have tended to rely on the notion of an ionization cutoff (for example, Ho and Arons 1987; Blondin *et al.* 1990). In these models of MXRB systems, the wind velocity law (or correspondingly the radiative force) is assumed to be the same as that for a single star up until a point in the flow where the ionization parameter ξ (see § IIc) is equal to the cutoff value ξ_{cr} ($\log_{10} \xi_{cr} = 2.5$, Blondin *et al.* 1990; $\log_{10} \xi_{cr} = 4$, Ho and Arons 1987). At this point, the radiative force is completely turned off and the wind coasts toward the neutron star.

The only other attempt to calculate the effect of X-ray ionization on the line force, comparable to the present paper, has been that by MacGregor and Vitello (1982, hereafter MV). MV calculated the wind dynamics along the line of centers of a MXRB system, including the effect of the X-rays from the neutron star on the temperature and ionization structure of the wind, and the subsequent change in the radiative force and wind dynamics. This work, however, has some serious limitations. In terms of the radiative line force, MV only included the contributions from a total of 15 lines from the ionic species C III–IV, N III–V, and O III–VI. MV published only three models for varying L_x, the X-ray luminosity of the neutron star (namely $L_x = 0$, 10^{33}, and 10^{34} ergs s^{-1}). At values of L_x greater than about 5×10^{34} ergs s^{-1}, MV found that mass loss from the primary was completely extinguished, a results at

[1] NAS/NRC research associate.

odds with observations of MXRB systems with X-ray luminosities greater than 10^{36} ergs s^{-1}.

Also of relevance is the work by Masai (1984) concerning the structure of X-ray irradiated stellar winds. Masai (1984) considered, in a rudimentary way, the consequences of including optical depth effects in the stellar wind, particularly opacity associated with He II, finding these effects to be reasonably significant. Masai (1984) did not, however, attempt self-consistent models of MXRBs. The problems associated with optical depth effects will be discussed at much greater length later in the paper (see § IV*a*).

The motivation for this work lies in calculating reliable radiative force multipliers for the stellar wind in MXRB systems, including both the effects of X-ray ionization and heating. The resultant force multipliers $M(t)$ will now not only be a function of the optical depth parameter t as per CAK, but now also a function of the ionization parameter ξ, and will often be referred to, interchangeably, as $M(t, \xi)$. Also, these calculations will show that the force multiplier $M(t, \xi)$ does not exhibit the sharp cutoff previously assumed, but instead the decline is more gradual and much more complicated. These calculations will also show that a much larger number of lines contribute significantly to the total line force than assumed by MV. These results will enable the construction of more realistic, self-consistent dynamical models of MXRB systems.

The paper is organised as follows: first (§ II), the theory of the radiative line force multiplier calculations will be set out; next (§ III) the results of the calculations for a range of ionization conditions will be presented, and then the results and the implications of some of the assumptions will be discussed, as well as a brief look at some of the dynamical considerations that result from this work (§ IV). Most of the discussion concerning the dynamics of MXRBs will be deferred to a subsequent paper. The main conclusions of this work are briefly summarized in § V.

II. THE RADIATION FORCE

a) The Line Force

As was shown by Castor (1974), in a radially expanding atmosphere where the velocity gradient is assumed to be large, a given spectral line contributes a net force per unit mass to the stellar wind material given by

$$f_L = \left(\frac{\Delta v_D F_v}{c}\right)\left(\frac{\kappa_L}{\tau_L}\right)(1 - e^{-\tau_L}) , \tag{1}$$

where Δv_D is the Doppler width of the transition ($= vv_{th}/c$, v_{th} defined as the thermal speed of a hydrogen atom, Abbott 1982), F_v is the emitted flux of the stellar core, τ_L is the line optical depth, and κ_L is the monochromatic line opacity per unit mass, such that

$$\kappa_L = \frac{\pi e^2}{m_e c} gf \frac{N_L/g_L - N_U/g_U}{\rho \Delta v_D} , \tag{2}$$

where N_L, g_L and N_u, g_U are the respective populations and statistical weights of the upper and lower levels of the transitions.

In a rapidly expanding stellar wind, where the velocity gradient is assumed to be large, the line optical depth in the radial direction can be reduced from a integral representation to a purely local quantity (Castor 1974)

$$\tau_L = \int_r^\infty \phi \rho \kappa_L \, dr = \frac{\rho v_{th} \kappa_L}{dv/dr} , \tag{3}$$

where ϕ is the line profile. The result given in equation (3) essentially comprises the mass of a column of gas over which the velocity changes by a Doppler width $[\rho v_{th}/(dv/dr)]$ multiplied with the optical depth per unit mass (κ_L).

Following CAK, it is useful to define two new variables

$$t = \sigma_e v_{th} \rho \left(\frac{dv}{dr}\right)^{-1} , \tag{4}$$

such that t is a local optical depth parameter (see eq. [3]), and

$$\eta = \frac{\kappa_L}{\sigma_e} , \tag{5}$$

such that η is the ratio of the line opacity coefficient to the electron-scattering coefficient σ_e. Then, as a consequence

$$\tau_L = \eta t . \tag{6}$$

Summing the individual line forces f_L over all lines leads to the result that the total radiative line acceleration a_L is given by

$$a_L = \frac{\sigma_e F}{c} M(t) , \tag{7}$$

where F is the frequency integrated flux from the stellar atmosphere. The term $\sigma_e F/c$ refers to the force due to continuum radiation pressure, while $M(t)$, which is termed the force multiplier, is a convenient means of parameterizing the force due to the lines, and is given by

$$M(t) = \sum_{\text{lines}} \frac{\Delta v_D F_v}{F} \frac{1}{t} (1 - e^{-\eta t}) . \tag{8}$$

Also, the force multiplier for an individual line is designated $M_L(t)$. Thus, from equation (8), transitions which have energies close to the maximum of the stellar flux will tend to dominate the total line force.

There exist two separate asymptotic limits to the force associated with an individual line. In the optically thin case $\tau_L \ll 1$, equation (1) reduces to

$$f_L = \left(\frac{\Delta v_D F_v}{c}\right)(\sigma_e \eta) , \tag{9}$$

and in the optically thick limit $\tau_L \gg 1$

$$f_L = \left(\frac{\Delta v_D F_v}{c}\right)\left(\frac{\sigma_e}{t}\right) . \tag{10}$$

Thus, in the optically thin limit the line force becomes independent of t and therefore independent of the wind dynamics. In the optically thick case, the line force becomes independent of η and independent of the line strength, and, in addition, is proportional to t^{-1}. The terms optically thick and thin used here refer only to the line optical depths; for a further discussion of the effects of a large continuum optical depth, see § IV*a*.

The equations derived here for the radiative line acceleration are, strictly speaking, only applicable for the cases where the radiation field of the mass-driving star is assumed to stream radially, and no account has been made of the finite disk of the star. The generalization to the case where the finite disk factor is included is straightforward, and, in essence, the problem, can be reduced to simply multiplying the force multiplier $M(t)$ by the dynamical correction factor termed $K(r, v, dv/dr)$ (Pauldrach, Puls, and Kudritzki 1986). The calculation of the finite disk correction factor will be dealt with in a subsequent paper. Given these assumptions, for given ionic abundances

and excitation conditions, and knowing the frequency and strength of the radiative transitions for all considered species, the line force multiplier $M(t)$ can be readily calculated.

Abbott (1980, 1982) has given an excellent review of some of the assumptions inherent in the equations given above and their potential effect on the force multiplier for the case of a wind from a single star, and they will not be reproduced here. Some specific problems associated with the line force calculations in the case of winds in MXRB systems will be dealt with later (§ IV*a*).

b) Atomic Data

As demonstrated by Abbott (1982), the total radiative line force is potentially made up of contributions from a very large number of transitions from a wide range of ionic species. Therefore, in order to calculate the line force, a correspondingly large amount of atomic data is required. In these calculations, the line list described by Abbott (1982) is utilized. This compilation of data contains approximately 250,000 *gf*-values for transitions from over 17,000 different electronic levels, and is essentially complete for the first six ionization stages for the first 30 elements (i.e., H to Zn). For the case of stellar wind material ionized only by the radiation field of the primary, this is sufficient, there being no significant amounts of any ionic species more highly ionized than this. However, in the case of an MXRB, there will be a strong flux of high-energy photons sufficient to produce highly ionized species over much of the flow, and indeed, close to the neutron star, the wind material will be almost completely stripped of electrons. Therefore, in order to model the effects of the X-ray ionization on the line force, extensions to this line list must be made. However, the atomic data are almost completely lacking for many highly ionized ionic species, and it is necessary to resort to scaling along isoelectronic sequences to obtain the necessary data.

For hydrogenic species (neglecting relativistic corrections which become important for elements with high Z), the wavelengths of the transitions are given by $\lambda_Z = Z^{-2}\lambda_H$, with λ_H the wavelength of the transition in the hydrogen atom, and λ_Z the wavelength of the transition in a hydrogenic ion with atomic number Z, and for the f-values $f_Z = f_H$ (see Reader *et al.* 1980). For nonhydrogenic species, the oscillator strengths for a particular transition still behave in a systematic way along isoelectronic sequences, though the behavior is not as simple as for hydrogenic species (Smith and Wiese 1971).

For simplicity, the wavelengths and oscillator strengths for the transitions for all ionic species where the data is not available have been assumed to scale as for hydrogenic species, so, for example, the contribution to the force multiplier from Fe XVII (a neon-like species) is represented by that of Ar IX (for which data are available in the Abbott 1982 line list) with transition wavelengths and oscillator strengths scaled as above.

Having to represent certain ions in this manner is not expected to be a major source of error, because the energies of the major transitions of the ions for which interpolation is necessary tend to lie at values significantly greater than the peak of the stellar flux and will not contribute greatly to the force multiplier (see eq. [8]). Also, comparison calculations made for specific ions with the limited data compilation of Reader *et al.* (1980) support the assertion that the scaling required in the atomic data will not be a major source of error.

c) Ionization Balance

In an optically thin gas, for a given spectral shape, the ionization and thermal structure of the gas is determined solely by the ionization parameter ξ (Tarter, Tucker, and Salpeter 1969) given by

$$\xi = \frac{L_x}{n_n r_x^2}, \tag{11}$$

where L_x is the X-ray luminosity of the source, n_n is the nucleon number density of the gas, and r_x is the distance from the X-ray source.

While, in reality, optical depth effects are likely to play a role in the winds of MXRBs, the problem of realistically calculating the radiative transfer makes the problem beyond the scope of this paper. Their inclusion will lead to, among other things, further coupling between the wind solution and the resultant X-ray luminosity. For the purposes of these calculations, the wind will be assumed to be optically thin; optical depth effects will be discussed at greater length later in § IV*a*.

The photoionization code described by Kallman and McCray (1982) has been utilized to calculate the ionization structure in the wind. This code calculates the ionization balance and thermal structure over a wide range of physical conditions, and it includes a total of 13 elements, namely H, He, C, N, O, Ne, Mg, Si, S, Ar, Ca, Fe, and Ni, with the element abundances taken from Cameron (1973). Also, as in the MXRB model calculations of McCray *et al.* (1984), a lower limit is set on the gas temperature T, namely $T \geq T_*$ with T_* being the effective temperature of the primary, which in this case is $T_* = 25{,}000$ K (appropriate for the archetypal MXRB Vela X-1). At higher values of ξ, the gas temperature can rise to $T \geq 10^7$ K (see Kallman and McCray 1982). A bremsstrahlung-type spectrum has been assumed for the radiation field of the neutron star, with a characteristic temperature of $kT_x = 10$ keV, with no low-energy cutoff, appropriate for this type of object (White, Swank, and Holt 1983; see also § IV*a*).

In order to include the contributions to the radiative line force from the other 17 elements with $Z \leq 30$, which are included in the line list calculations but which are not included in the photoionization calculations (and for which, for the most part, sufficient atomic data do not exist to reliably calculate the ionization structure), it has again been necessary to scale along isoelectronic species to find the ionization balance for these elements. For a given value of the ionization parameter ξ, the abundances of ionic species on a given isoelectronic sequence follow a systematic pattern as a function of Z, and from these values it is straightforward to interpolate the abundances of the species for which the ionization structure is not calculated. Also, because the species which are not accounted for in the photoionization code are those with the smaller abundances, they tend not to contribute significantly to the total line force multiplier (typically less than 5% of the total force multiplier, with Al and P being the major contributory elements). Numerical experiments have verified that errors in the force multiplier $M(t)$ associated with the interpolation of ion fractions for these elements are likely less than 2%–3%, and, as such, are not considered a major source of error.

d) Excitation Structure

In order to calculate the force multiplier $M(t)$, it is necessary to make some assumptions concerning the excitation conditions of the wind material, and in these calculations the wind

material has been assumed to be in LTE, and the excitation structure to be given by the Boltzmann equation.

For the case of a single star, Abbot (1982) used the results of detailed statistical equilibrium calculations of H and He in an expanding atmosphere by Klein and Castor (1978) to justify the use of the Boltzmann distribution. This assumption is less likely to be valid for trace ions, particularly the very highly ionized species which may be produced by X-ray ionization. However, a more accurate treatment of the excitation would require the calculation of the populations of 10^5 atomic levels, which is beyond the scope of this paper. Some of the consequences and likely errors which result from the assumption of LTE are discussed in § IV*a*.

III. FORCE MULTIPLIER RESULTS

The radiative force multiplier $M(t, \xi)$ has been calculated on a grid of t-values from $t = 10^{-8}$–10^{0}, for values of the ionization parameter ξ ranging from $\xi = 0$–10^4. These values should provide an ample range of results for any models of massive X-ray binary systems. The primary star, the radiation field of which enters in through equation (1), has been represented by a Kurucz model atmosphere with an effective temperature of $T_* = 25{,}000$ K and an effective gravity of $\log g = 3.0$, values appropriate for the B0 I primary of Vela X-1. As was also found by Abbott (1982), the force multiplier results are reasonably insensitive to the precise value of $\log g$.

Abbott (1982) introduced an additional dependency for the force multiplier $M(t)$ on the density of the material (more specifically on n_e/W, n_e being the electron density, and W being the dilution factor of the stellar radiation field). The calculations for the case of the single-star model in question here (i.e., with $\xi = 0$) found a similar weak dependence in the force multiplier on the density, $M(t) \propto (n_e/W)^{0.06}$. However, at higher values of ξ the density dependence quickly disappeared, and all the results presented in the remainder of the paper will be for a single density ($n_e/W = 4 \times 10^{10}$ cm^{-3}). Even in the case of single-star models, the introduction of the density dependence does not significantly alter the wind dynamics.

In Figure 1, the dependence of the force multiplier $M(t, \xi)$ with t is shown for a number of representative values of ξ. For values of $t \leq 10^{-8}$ the line force is roughly constant, all lines being optically thin (i.e., $\tau_L = \eta t \ll 1$), and the line force then being independent of t. For large values of t, the line force becomes much smaller than the continuum radiative force and ceases to have any significant dynamical role. Figure 2 also illustrates the behavior of $M(t)$ with ξ, but this time concentrating on the variation of $M(t)$ with ξ for four different values of t.

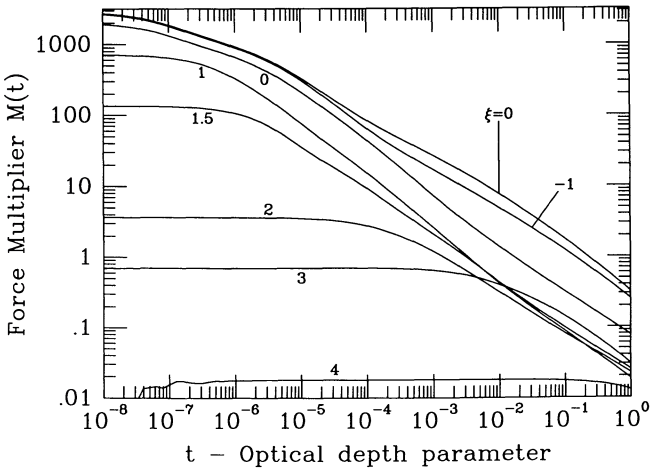

FIG. 1.—Suppression of the radiative force multiplier $M(t)$ with increasing X-ray ionization. $M(t)$ is plotted as a function of the optical depth parameter t for a number of different values of the ionization parameter ξ. The curves are labeled with the respective value of $\log_{10} \xi$, except for the case of $\xi = 0$.

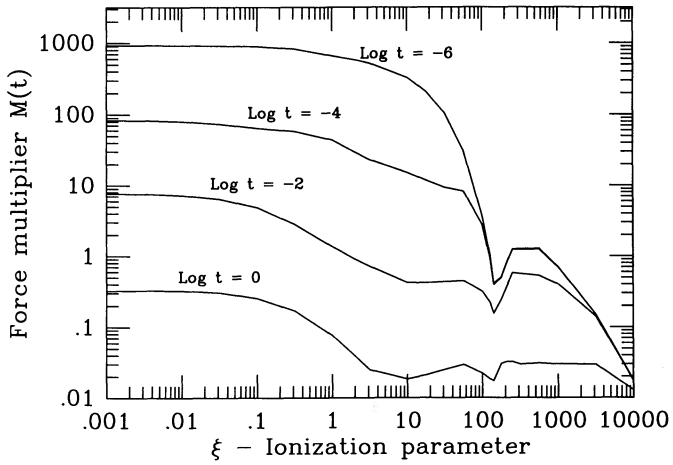

FIG. 2.—Suppression of the radiative force multiplier $M(t)$ with increasing ionization. This time, $M(t)$ is plotted as a function of the ionization parameter ξ for different values of the optical depth parameter t. The curves are labeled with their respective value of t.

There are several important points to note from Figures 1 and 2. As would be expected, at lower values of ξ, the X-ray flux is weak, and does not greatly alter the state of the gas. Consequently, the force multiplier is essentially unchanged at all values of t, and shows the basic power-law relationship between $M(t)$ and t that was found by CAK. At higher values of ξ the force multiplier displays a more complex behaviour. The general trend is for $M(t)$ to decrease as ξ increases, and while the behaviour is qualitatively the same for all values of t, it is quantitatively different. The force multiplier $M(t)$ is more susceptible to change for higher values of t, with significant relative reductions in $M(t)$ occurring at lower values of ξ for higher values of t. Also, at higher ξ, the force multipliers $M(t)$ begin to show a distinct turnover at smaller values of t, where $M(t)$ becomes independent of t. The location of this turnover extends to higher and higher values of t as ξ increases. Another important point is that the gradient of $M(t)$ at the higher values of t (i.e., at values of t greater than the point at which the value of the force multiplier becomes independent of t) is, to a reasonable approximation, constant with ξ.

To understand further what is causing this behavior in X-ray illuminated stellar winds, it is useful to compare with the case of a single star. Abbott (1982) has calculated the force multiplier as a function of the effective temperature $T_{\rm eff}$ of the star, finding that $M(t)$ was largely insensitive to $T_{\rm eff}$, for a wide range of values of $T_{\rm eff}$. This behavior is a consequence of the radiation field of the primary determining the ionization balance, and which in turn determines the force multiplier. Following the argument from Abbott (1982), in the winds of OB stars, the dominant ionization state of an element has an ionization potential of around 20–30kT, the wavelengths of the major resonance lines of this species will typically correspond to energies of one-quarter of the ionization potential (i.e., around 5–7kT), while the maximum of the function vB_ν occurs

at $4kT$, and this correlation tends to keep the force multiplier remarkably constant. However, in an X-ray binary system, this is not necessarily the case; at higher values of ξ the ionization and thermal structure of the wind is essentially determined by the radiation field of the neutron star. In MXRBs the wind material will always be over ionized compared to the case of a single star, and this generally leads to ionic species dominating in the wind, which tend to have important lines at energies considerably higher than the maximum point of the flux distribution of the primary star. Thus, X-ray ionization tends to remove the ions that provide most of the line force. While strong lines from highly ionized species which do not exist in the absence of an X-ray source, such as O VI and O VIII, can significantly contribute to $M(t)$ at higher values of ξ (see Table 1 and Figs. 3 and 4), this does not counteract the overall decline. From equation (10), as a driving line becomes optically thick ($\tau_L = \eta t \gg 1$), the contribution to the radiative force from that line levels out, and further increases in τ_L do not increase the radiative force, so that the addition of a few strong lines cannot offset the removal of a large number of strong driving lines.

TABLE 1

INDIVIDUAL RADIATIVE LINE FORCE MULTIPLIERS $M_L(t)$ AND LINE OPTICAL DEPTH τ_L FOR THE STRONGEST DRIVING LINES FOR DIFFERENT VALUES OF THE IONIZATION PARAMETER ξ

Ion	λ(Å)	$\tau_L(t = 10^{-4})$	$M_L(t = 10^{-4})$
	$\xi = 0$		
C III	1247.4	6.52	0.844
Si III	1113.2	64.96	0.843
Si III	1113.2	11.73	0.843
Si III	1110.0	34.71	0.843
Si III	1109.9	11.87	0.843
Si III	1108.4	15.99	0.843
C II	1036.3	24.13	0.835
N II	1085.7	62.47	0.835
	$\log_{10} \xi = 0$		
N V	1242.8	15.34	0.845
N V	1238.8	30.59	0.844
C III	1247.4	5.44	0.842
Si III	1113.2	5.55	0.840
C II	1036.3	10.25	0.835
	$\log_{10} \xi = 1$		
N V	1242.8	25.96	0.931
N V	1238.8	51.75	0.930
O VI	1037.6	183.83	0.917
O VI	1031.9	380.88	0.897
C III	1175.6	11.51	0.854
	$\log_{10} \xi = 2$		
He II	1640.0	0.996	0.720
O VI	1031.9	0.288	0.486
O VI	1037.6	0.139	0.258
He II	1214.8	0.169	0.246
He II	4685.8	1.929	0.168
	$\log_{10} \xi = 3$		
O VIII	1164.8	0.018	0.116
O VIII	1931.7	0.028	0.081
O VIII	2976.4	0.042	0.062
O VIII	4341.3	0.060	0.042
O VIII	6069.2	0.082	0.026
	$\log_{10} \xi = 4$		
S XVI	1085.3	0.0001	0.0015
S XVI	2050.7	0.0002	0.0012
S XVI	1517.3	0.0001	0.0012
Si XIV	1417.6	0.0001	0.0011
Ca XX	1312.5	0.0001	0.0011

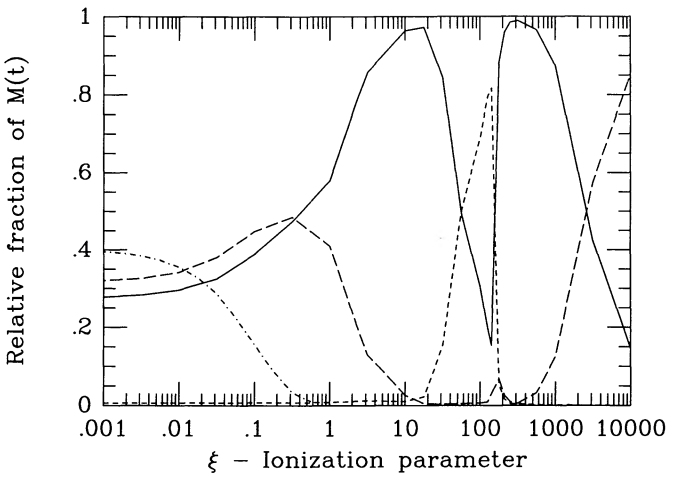

FIG. 3.—Relative force contributions from different atomic species for $t = 10^{-4}$. The elements have been binned into four groups: (*i*) H to He (*small dashed line*), (*ii*) Li to F (*full line*), (*iii*) Ne to Ca (*large dashed line*), and (*iv*) Sc to Fe (*dot-dashed line*). See text for further details.

The turnover in $M(t)$ at lower values of t is a consequence of there being less optically thick lines at these values of t with increasing ξ. From equation (8), $M_L(t)$ becomes independent of t for optically thin lines. Also, as more highly ionized species tend to have less strong lines than less ionized species, increasing ionization tends to reduce the number of optically thick lines. Thus, for higher ξ the extent of the region where $M(t)$ is independent of t increases to higher values of t.

The temperature increase which occurs with ξ also affects the force multiplier. For a given line, the force multiplier for that line depends on the gas temperature T, namely that $M_L(t) \propto T^{1/2}$ (eq. [1]). While this can raise the contribution from individual lines (see Fig. 4), when coupled with the depen-

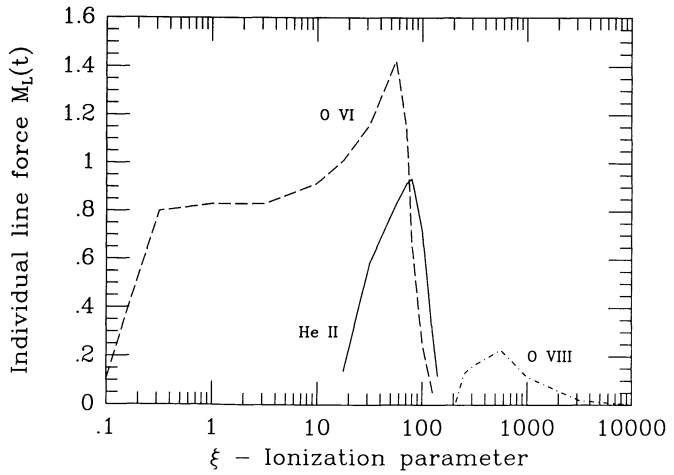

FIG. 4.—Force multipliers $M_L(t)$ for three individual lines, as a function of ξ, for $t = 10^{-4}$. The lines shown are O VI λ1038 (*dashed line*), O VIII λ1165 (*dot-dashed line*), and He II λ1640 (*full line*).

dence of the ionization structure on ξ, this again cannot offset the decline of $M(t)$ with ξ.

From Figure 2, at values of ξ around $\log_{10} \xi = 2$, there is an interesting decline and subsequent increase of $M(t)$ with increasing ξ, which, while present at all t, is more marked for smaller values of t. The behavior around $\log_{10} \xi = 2$ is largely related to the contribution of certain lines from highly ionized species of oxygen, and in particular lines of O VI and O VIII (note that the relevant lines of O VIII, which is a hydrogenic species, correspond to the Pfund series).

To further illustrate this, the relative contributions of the various elements have been plotted as a function of ξ. The elements have been grouped together into four bins, namely: (*i*) H and He , (*ii*) Li to F (where the main contributions will come from C, N, and O), (*iii*) Ne to Ca, and (*iv*) Sc to Zn (with Fe being the main contributor). In Figure 3, the relative contributions for each of these bins is plotted as a function of ξ (note that the results in Fig. 3 are for the case of $t = 10^{-4}$). At low ξ, bins (*ii*)–(*iv*) each contribute very roughly around one-third (in agreement with the results of Abbott 1982), with H and He contributing very little for most values of ξ. As ξ increases, the relative contribution from the Fe type elements drops rapidly and does not contribute significantly for $\log_{10} \xi \geq -1$. The elements Ne-Ca, along with the C, N, and O elements, dominate the force multiplier for most values of ξ. Ne-Ca eventually stops being a major contributor at $\log_{10} \xi = 1$, but, at very high values of ξ, it returns to being the major contributor (mainly from hydrogenic Si and S, see Table 1). At values of $\log_{10} \xi$ between 0.5 and 1.5, lines of N V and O VI dominate $M(t)$, and for $\log_{10} \xi$ between 2.5 and 3.5, lines from O VIII dominate. However, close to $\log_{10} \xi = 2$, the relative contribution from O VI and N V falls rapidly as the abundances of these ions drop sharply as the material becomes increasingly ionized. This coincides with a sharp increase in the force associated with He II λ1640. At this point He is mostly fully ionized, but the high temperature can populate the appropriate excitation levels of the singly ionized species and this, coupled with the temperature dependence of $M_L(t)$, can lead to a sharp rise in $M_L(t)$ for the He II λ1640 line. This results in the sudden increase in the relative contribution from H and He seen in Figure 3 and the sharp decline in the relative contribution from C, N, and O close to $\log_{10} \xi = 2$. This is further illustrated in Figure 4, where the variation of the force multiplier $M_L(t)$ of three relevant individual lines with the ionization parameter are plotted (again for the case of $t = 10^{-4}$. The three lines shown in Figure 4 are O VI λ1038, O VIII λ1165, and He II λ1640. In Figure 4, at low values of ξ, none of the lines in question contribute significantly to $M(t)$. As the degree of ionization increases, the population of O VI increases, and the force contribution increases linearly, and finally levels off as the line becomes optically thick. At higher ξ, as the temperature begins to sharply increase, the force contribution from O VI λ1032 and He II λ1640 both increase (eq. [8]). However, the populations of these ions begin to decrease sharply at this point, the lines desaturate, and the force contributions from both lines drop sharply. Also, the population of O VIII begins to rise and begins to significantly contribute to the force multiplier. Finally, at even higher ξ, even the population of O VIII becomes insignificant and the line force associated with it drops off.

In Table 1, the strongest driving lines are given for a range of different values of ξ. The table reveals the trend that, for higher levels of ionization, the radiative driving comes from more highly ionized species. Table 1 also shows the trend that the line optical depths and the line force drops with increasing ξ, as has been shown in previous diagrams. It also shows that lines of certain more highly ionized species, such as O VI and N V, can have very high optical depths and individual line force multipliers $M_L(t)$ even at relatively high values of ξ (see also Fig. 4). Table 1 also shows that at very high values of ξ, hydrogenic species are essentially the only ones to contribute to the line force.

Comparison of Table 1 with Figure 2 gives an indication of the contribution of the strongest individual lines to the total force multiplier. At lower ξ, the total line force is made up from the contribution of many hundreds of lines, with no one lines contributing more than 1% of the total force multiplier. As ξ increases, the number of lines significantly contributing to the line force drops, though the contribution of the strongest line to $M(t)$ is still usually less than 5%–10%. The exceptions to this occur around $\log_{10} \xi = 2$, when the He II λ1640 line contributes over 20% of $M(t)$, and around $\log_{10} \xi = 3$ when the O VIII λ1165 line contributes over 15% of $M(t)$.

a) Parameterizing the Results

CAK showed that their force multiplier expression ($M(t) = kt^{-\alpha}$) could be reproduced by assuming a simple statistical model of the distribution of lines in both strength and frequency, namely that the logarithm of the line frequencies are uniformly distributed, and the line strength parameter η is distributed as a power law, so that the number of lines dN in an interval dv and $d\eta$ is given by

$$dN = -N_0 \eta^{\alpha - 2} d\eta \frac{dv}{v}, \tag{12}$$

where η is the line strength parameter (see eq. [5]), N_0 is a normalizing constant, and α is the CAK constant. (Note that CAK used β to parameterize the line strength, with β being the inverse of η, but apart from this the expressions are equivalent.)

Putting this expression into equation (8) and converting the summation into an integral over v and η, leads to the CAK result for the force multiplier (i.e., $M(t) = kt^{-\alpha}$) with

$$k = \frac{v_{\rm th}}{c} \frac{N_0 \Gamma(\alpha)}{(1 - \alpha)}, \tag{13}$$

where $\Gamma(\alpha)$ is the complete gamma function. Owocki, Castor, and Rybicki (1988, hereafter OCR) introduced a further refinement to this representation of the line force which helps parameterize the force multiplier results shown in Figures 1 and 2. Instead of using the power-law relationship for statistical distribution of the line strengths in equation (12), OCR modified this to be an exponentially truncated power law, namely

$$dN = -N_0 \eta^{\alpha - 2} e^{-\eta/\eta_{\rm max}} d\eta \frac{dv}{v}, \tag{14}$$

where $\eta_{\rm max}$ is a cutoff to the maximum line strength.

By the same procedure as above, substitution of this expression into equation (8) and integrating yeilds a modified form for the force multiplier

$$M(t) = \left[\frac{v_{\rm th}}{c} \frac{N_0 \Gamma(\alpha)}{(1 - \alpha)}\right] t^{-\alpha} \left[\frac{(1 + \tau_{\rm max})^{1-\alpha} - 1}{\tau_{\rm max}^{1-\alpha}}\right], \tag{15}$$

where $\tau_{\rm max} = t\eta_{\rm max}$. This again has a similar form as $M(t) = kt^{-\alpha}$. but this time with an additional correction factor.

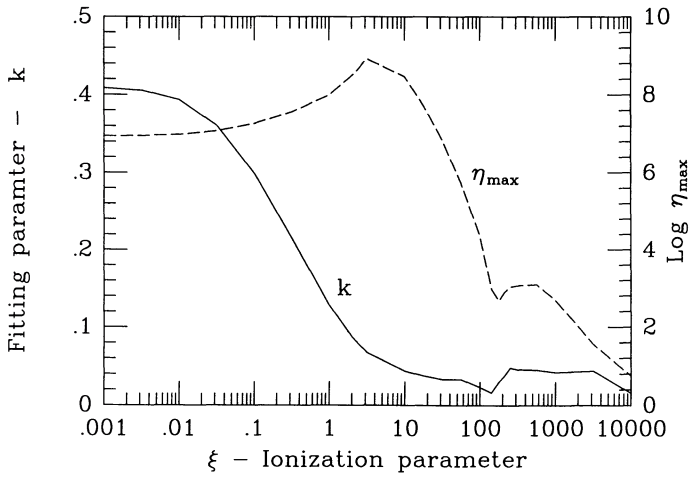

FIG. 5.—Best fit parameters for the force multipliers $M(t, \xi)$. Shown are the results for the parameter k (*full line*) and the parameter η_{max} (*dashed line*).

Note that this correction factor has asymptotic limits for both large and small values of τ_{max}, namely

$$\left[\frac{(1+\tau_{max})^{1-\alpha}-1}{\tau_{max}^{1-\alpha}}\right] = \begin{cases}(1-\alpha)\tau_{max}^{\alpha}, & \tau_{max} \ll 1 , \\ 1, & \tau_{max} \gg 1 . \end{cases} \quad (16)$$

At large τ_{max}, equation (15) reduces to the CAK power-law relationship, while at small τ_{max}, the force multiplier becomes independent of t, and

$$\lim_{\tau_{max}\to 0} M(t) = (1-\alpha)k\eta_{max}^{\alpha} , \quad (17)$$

where k is given by equation (13), which mimics the behaviour of the force multipliers found earlier (§ III).

Inspection of Figure 1 shows that at higher values of t, in general, the slope of the force multiplier is largely unchanged and stays close to a value of $\alpha = 0.6$. Thus, to a reasonable approximation, it can be assumed that α is constant throughout, and the only variations in $M(t)$ can be accounted for in terms of k and η_{max} (see eq. [15]).

Least-squares fits, using the parameterization shown in equation (15), have been made to the force multiplier results shown in Figure 1, with k and η_{max} being the two relevant parameters. In Figure 5, the results for the best fit values of (k, η_{max}) as a function of ξ are shown. The fits for $M(t)$ for each value of ξ are typically accurate to about 5% or 10%, and the worse errors are within a factor of 2. Better fits could have been found by also allowing the value of α to vary as a function of ξ, but it was felt that doing so would reduce the usefulness of the results in future models using a CAK type formulation.

In addition, in the regime of $\log_{10} \xi \leq 2$ (see § IV*a*), the fitting parameter k and η_{max} can in turn be fitted with the following exponential functions of ξ only:

$$k = 0.03 + 0.385 \exp(-1.4\xi^{0.6}) , \quad (18)$$

and

$$\log_{10}\eta_{max} = \begin{cases}6.9 \exp(0.16\xi^{0.4}), & \log_{10}\xi \leq 0.5 , \\ 9.1 \exp(-7.96\times 10^{-3}\xi), & \log_{10}\xi > 0.5 . \end{cases} \quad (19)$$

Thus, the very complicated behaviour of $M(t)$ with ξ seen in Figures 1 and 2, can be reduced to an analytic function of ξ. Using the analytic formulae for k and η_{max} somewhat reduces the accuracy of the representation of $M(t)$, but, for typical wind models, the accuracy of the fits is still within a factor of 2 for the appropriate values of ξ and t.

IV. DISCUSSION

a) Limitations

A number of important limitations inherent in the calculations presented here should be noted.

i) *Optical Depth Effects*

In the above calculations, all optical depth effects in the transfer of the radiation field of the neutron star through the wind material have been neglected, and the ionization structure used in the force multiplier calculations has been calculated, assuming the material is optically thin. In actual MXRB systems, this condition will likely be violated for portions of the flow (note that, while in the force multiplier calculations individual lines were frequently found to be optically thick, that is $\tau_L \gg 1$; this is different from allowing for optical depth effects with respect to the radiation field of the neutron star).

The inclusion of optical depth effects in self-consistent models of MXRBs remains a formidable, and as yet unsolved, problem. With respect to the approach developed here, optical depth effects will alter the thermal and ionization structure of the wind (the extent to which it does will depend largely on N_H, the column density of material between the neutron star, and the point in the wind under consideration); in turn, this will affect the force multiplier $M(t)$, and this, in turn, modifying the wind dynamics, and thus feeding back to change the column density of material blocking the flux from the neutron star, the end result being to make the problem even more coupled.

In an MXRB, for a specific value of ξ, the inclusion of transfer affects will tend to make the wind less ionized than it would be otherwise, the wind material blocking out some of the ionizing flux. Also, the ionization fronts will be much steeper in optically thick material, and the temperature structure will also be altered (see Kallman and McCray 1982). In general, the fact that material is less ionized will tend to make the radiative force multiplier greater than it would have been in the optically thin case.

In a stellar wind of an early-type star, the total wind column density N_H is large, typically around 10^{24} cm^{-2} (in most CAK type models, one of the boundary conditions is usually to set the total electron scattering optical depth in the wind to unity). However, a large fraction of the contribution to the total column density N_H will occur in close to the primary star (where the wind density is much higher), and the typical column density of material from, for example, $1.1R_*$ to a typical radius of the neutron star orbit ($\sim 2\ R_*$) is more characteristically around 10^{22} cm^{-2}. However, even at these columns, as will be shown below, optical depth effects can still be appreciable. Thus, very high column densities ($N_H \geq 10^{24}$ cm^{-2}) from the neutron star will only occur in the lower velocity regimes of the flow, where the density is high, and ξ is low, and from Figures 1 and 2, for these conditions, the X-rays from the neutron star will not significantly alter the value of $M(t)$, and the neglect of optical depth effects will not be important. Also, at values of $\log_{10}\xi \geq 2$, the results of Kallman and McCray (1982) demonstrate that optical depth effects will not be important in this regime either. Optical depth effects are thus likely only to play a significant role for intermediate values of ξ (i.e., $-1 \leq \log_{10}\xi \leq 2$).

To illustrate this, force multipliers $M(t)$ have been calculated allowing for optical depth effects in a simplified manner, for specific values of ξ, and N_H. In the optically thin case, the ionization structure and thermal structure of the wind material is determined solely by the ionization parameter ξ. When optical depth effects are included, to a reasonable approximation, the ionization and thermal structure now depend on ξ, and the column density of absorbing material N_H. The magnitude of optical depth effects have been estimated by calculating the ionization and thermal structure the wind material after the incident radiation field of the neutron star has been transferred through a slab of material of uniform density (with $n = 10^{11}$ cm^{-3}, n being the atomic number density of the slab material). This approach allows the determination of the ionization and thermal structure of wind material illuminated by an incident flux which has suffered absorption. From this, a force multiplier $M(t, \xi, N_H)$ can be calculated which accounts for, albeit in a simplified manner, the influence of a finite continuum optical depth on the radiative force multiplier. By varying the thickness of the slab, and the distance to the illuminating source r_x, the ionization and thermal state of the wind material can be determined for any particular value of ξ and N_H, and from this, as set out in § II, the force multiplier $M(t)$ can be calculated.

In Figure 6, two comparisons ahve been made to illustrate optical depth effects on the force multiplier calculations. The values of ξ and the column density N_H have been chosen to be approximately representative of conditions in a MXRB system (see § IV*b*). The two situations shown in Figure 6 are for the following cases: (*i*) $\log_{10} \xi = 0$, with $N_H = 0$ and 5×10^{22} cm^{-2}; and (*ii*) $\log_{10} \xi = 1$, with $N_H = 0$, and 10^{22} cm^{-2}.

In the first case, for $\log_{10} \xi = 1$, the difference between the optically thick and thin cases is less than a factor of 2 for all t. At low values of ξ, $M(t)$ is actually smaller in the optically thick case. However, the dynamical models in § IV*b* suggest that, for this value of ξ, the optical depth parameter t is likely to be in the range $t = 10^{-2}$–10^{-4}, and, for this range of t, the force multiplier in the optically thick case is typically between 50%–100% greater than for the optically thin case. In the second case, for $\log_{10} \xi = 0$, the column density of attenuating material is assumed to be a factor of 5 greater than in the first case. This additional column results in the wind material being significantly less ionized than in the optically thin case, and from this the force multiplier is larger than in the optically thin case for all values of t. The difference between the force multipliers in this case is always less than a factor of around 3, and for the values of t appropriate for the MXRB models in § IV*b*, the difference is between a factor of 2, and 3. The inclusion of optical depth effects has the result of shifting the force multiplier closer to the results for $\xi = 0$ (i.e., when there are no X-rays from the neutron star), a fraction of the ionizing radiation from the neutron star being blocked by the attenuating material. Thus, the inclusion of optical depth effects has the result of reducing the impact of the X-ray flux on the radiative driving in an X-ray illuminated stellar wind. Following on from this, X-ray induced dynamical effects will not become significant until higher values of ξ compared to optically thin models.

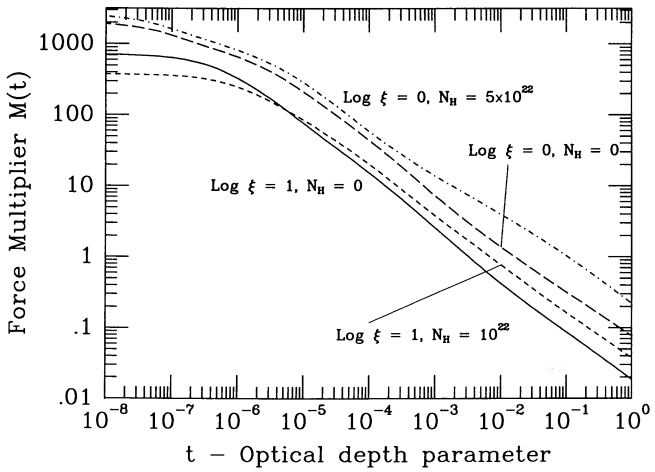

FIG. 6.—The influence of optical depth effects on the force multiplier $M(t)$. Results for $M(t)$ are given for the case of $\log_{10} \xi = 1$; optically thin (*full line*), and for a column density of $N_H = 10^{22}$ cm^{-2} (*short dashed line*). Also shown are results for $\log_{10} \xi = 0$; optically thin (*long dashed line*), and for a column density of $N_H = 5 \times 10^{22}$ cm^{-2} (*dot-dashed line*).

The conclusion of this section is that omission of optical depth effects will likely result in an underestimate of the force multiplier (possibly up to a factor 2–3) at certain points in the flow (see also § IV*b*). Though for large portions of the flow, the force multiplier results calculated with the optically thin approximation will be correct. Also, in several other types of systems where these calculations are applicable, such as the winds from accretion disks in cataclysmic variables, or in the Be/X-ray binary systems, the optically thin approximation will be appropriate (§ IV*c*).

ii) *Deviations from LTE*

One of the major assumption that has gone into these calculations is that the wind material is in LTE and that the excitation structure is given by the Boltzmann equation.

Abbott (1982) in his calculations for the winds of single stars was also forced to make the same assumption. However, by noting that, in expanding atmospheres, excited states with allowed radiative transitions to lower states are strongly underpopulated (Klein and Castor 1978), Abbott (1982) was able to justify the assumption of LTE in winds of single stars *a posteriori* by the fact that around 90% of the force came from lines arising from ground or metastable states.

In the force multiplier calculations presented in § III, at low values of ξ, a similar situation occurs, and for $\xi = 0$ roughly 90% of the force multiplier comes from lines arising in ground or metastable levels. As ξ increases, this situation still remains, for example, for $\log_{10} \xi = 1$ over 90% of the force multiplier still comes from lines arising in ground or metastable levels, while at $\log_{10} \xi = 1.5$ the contribution is still 75% of the force multiplier. However, at values of $\log_{10} \xi \geq 2$, the percentage of the force multiplier that comes from ground or metastable levels begins to decrease sharply [for $\log_{10} \xi = 2$, the contribution is 30% of $M(t)$, while for $\log_{10} \xi \geq 3$ the percentage is minimal], and, at these values of ξ, the assumption of LTE will lead to an overestimate of the force multiplier. However, this overestimation of the radiative force multiplier at values of $\log_{10} \xi \geq 2$ will likely not have a major impact on the dynamics of winds in MXRBs. The reason for this is as follows; in MXRB models, high values of ξ will only occur close to the neutron star (see eq. [11]), and close to the neutron star the dominant force will not be the radiative force, but will instead by the gravitational force of the neutron star. In the models presented in § IV*b*, at values of $\log_{10} \xi \geq 2$, the gravitational

force of the neutron star on the wind material is grater than the radiative force by more than one order of magnitude, even for the model with $L_x = 5 \times 10^{34}$ ergs s^{-1}, where the point at which $\log_{10} \xi = 2$ is furthest from the neutron star, and hence the gravitational force is the least. Therefore, the neglect in changes in the force multiplier resulting from deviations from LTE are unlikely to be a major source of error in MXRB models that use the force multipliers calculated in this paper.

iii) *Effects of the X-Ray Spectrum*

The results presented so far in this paper have been calculated only for a single spectrum, namely a 10 keV bremsstrahlung-type spectrum, and assuming a different spectrum will lead to quantitatively different force multipliers. Kallman and McCray (1982) have calculated the ionization and temperature structure for a variety of different spectra (i.e., blackbody, power-law, as well as bremsstrahlung). For example, X-rays are observed from single early-type stars, and are believed to be produced by shocks which form in the strongly unstable winds, and, in an analogous way to the case of X-rays binary systems, the X-rays will in turn modify the wind dynamics, though in this case an input spectrum such as those calculated by Krolik and Raymond (1985) might be more appropriate.

Also, as considered by MV, a low energy cutoff to the X-ray spectrum could have an effect on the radiative force. For the same X-ray luminosity and wind density, material irradiated by a spectrum with a deficiency of low-energy X-ray photons will be underionized compared to the case of a spectrum with no low-energy deficit. This is a result of the fact that the ionization thresholds for most ions considered fall at photon energies ≤ 1 keV, and because the ionization cross sections drop off roughly as E^{-3}, this can rapidly reduce the photoionization rate if the cutoff in spectrum is assumed to occur at a value higher than the ionization threshold for a particular ion.

This is illustrated in Figure 7, where force multipliers results are shown for the case of $\log_{10} \xi = 1$, but where the low-energy spectrum cutoff E_c is varied (see MV). For values of $E_c \geq 1$ keV, the X-rays have much less impact on the ionization structure of the wind, and thus $M(t)$ departs less from the case when $\xi = 0$. So the net result of a low-energy cutoff in the spectrum is to hold the value of $M(t)$ closer to the case of $\xi = 0$ until higher values of ξ are obtained than in the case of no low-energy cutoff. The difference this causes to the wind structure will not be discussed further here; however, it will result qualitatively in a decrease in the influence of the X-rays on the wind dynamics.

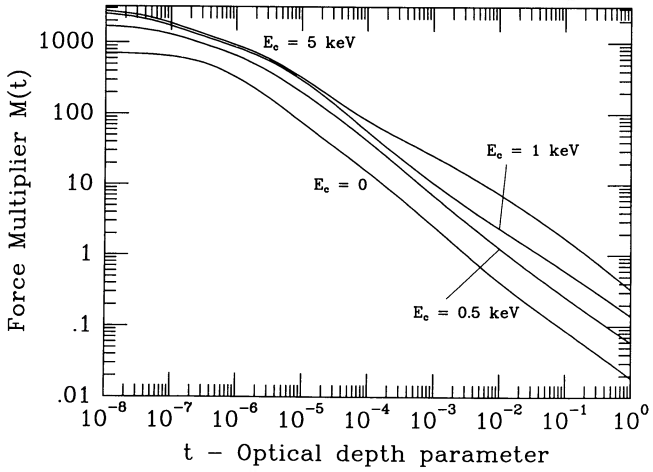

FIG. 7.—Effect on the force multiplier $M(t)$ of a low-energy cutoff in the assumed X-ray spectrum of the neutron star. The curves are labelled with E_c (in keV).

Similarly, increasing kT_x to 20 keV will also tend to increase $M(t)$ for a given value of ξ. Increasing kT_x means that there are less low-energy X-rays, and decreasing kT_x to, say 5 keV, will correspondingly decrease $M(t)$, there now being more softer X-ray photons, and the gas will be preferentially more ionized for the same ξ.

b) Dynamical Effects

The calculations presented earlier (§ III) are representative of the case of a MXRB system such as Vela X-1. While a more detailed treatment of the dynamical consequences of the behaviour of $M(t)$ with ξ will be deferred to a following paper, a brief outline will give given here.

Previous treatments of the effects of X-rays on the wind dynamics have assumed a sharp cutoff in the radiative force at a well-defined value of ξ (for example, Blondin *et al.* 1990; Ho and Arons 1987). These calculations have shown this not to be the case and that the decline of $M(t)$ with ξ is more gradual and indeed more complicated. On the basis of their calculations, both Ho and Arons (1987) and Blondin *et al.* (1990) derived some major conclusions; for example, Ho and Arons (1987) found the existence of two stable solutions for the wind dynamics and the resultant X-ray luminosity for MXRB systems, namely one low- and one high-luminosity state. Blondin *et al.* (1990) found that the effect of X-ray ionization created a high density wake that trailed behind the neutron star, causing enhanced absorption of the X-ray by wind material at certain phases, as has been seen in some MXRB systems (Kallman and White 1982). While a full discussion of whether or not these effects will still occur in dynamical models will be deferred to a subsequent paper, in Figure 8 wind solutions for MXRB models, which includes the effects of X-ray ionization and heating on the wind dynamics, are shown. For comparison, the wind solution for the case where the X-ray luminosity is assumed to be zero is also shown. The parameters for the primary star are assumed to be $R_* = 30\ R_\odot$, $M_* = 20\ M_\odot$, and $T_* = 25{,}000$ K. The neutron star is assumed to have a mass of $M_x = 1.4\ M_\odot$, and the system has been assumed to have a separation of $D = 60\ R_\odot$ or twice the radius of the primary (see MV). Figure 8 shows four model results, for X-ray luminosities of $L_x = 0$, 10^{33}, 10^{34}, and 5×10^{34} ergs s^{-1}.

For these models, the mass-loss rate is largely unaffected by the inclusion of the effect of X-rays. This is a consequence of the fact that, in CAK type models, the mass-loss rate is determined by conditions at the critical point. In these models, the critical point r_c lies at around $1.05\ R_\odot$, and at this radius $\log_{10} \xi_c \leq -2$, and the radiative force at the critical radius is largely unaffected (see Fig. 2), and, as a consequence, the mass-loss rate is also largely unaffected (see Table 2). However, in models with larger X-ray luminosities, potentially ξ_c can be sufficiently large to change the radiative force at the critical point, and thus, the overall mass-loss rate. Following on from this, therefore, the wind dynamics in the subsonic regime are also not signficantly altered. However, in the supersonic regime, the X-rays do cause significant alterations in the wind dynamics, the X-rays tending to suppress the radiative force and thus suppress the wind velocity. For the model with $L_x = 5 \times 10^{34}$ ergs s^{-1}, the wind velocity is held close to a value of 200 km s^{-1} for a large part of the flow. For the model with $L_x = 10^{34}$

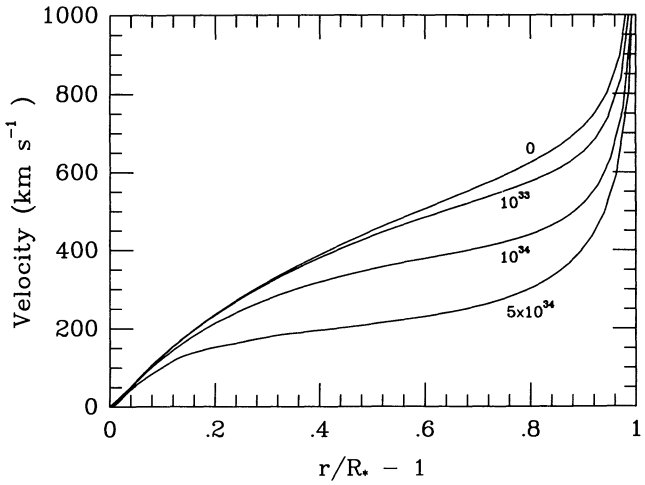

FIG. 8.—X-ray induced suppression of the wind velocity. The changes in the wind dynamics of an MXRB system caused by X-ray ionization, for values of the neutron star X-ray luminosity of $L_x = 0$, 10^{33}, 10^{34}, and 5×10^{34} ergs s^{-1}. The curves are labeled with the respective value of the X-ray luminosity. The neutron star lies at a radial distance of $r = 2\ R_*$.

ergs s^{-1}, the wind velocity is also suppressed in the supersonic regime, but by a correspondingly smaller amount. At locations in the wind close to the neutron star, the gravitational force of the neutron star becomes the dominant force, completely swamping the radiative line force contribution, and all models show a very steep increase in velocity near to the secondary. In Table 2, additional results from the model calculations are given.

The accretion radius for gravitational capture of material is given by

$$r_{\rm acc} = \frac{2GM_x}{v^2}, \qquad (20)$$

where M_x is the mass of the neutron star and v is the wind velocity, and thus, the accretion radius is a very sensitive function of the wind velocity. A typical value for the accretion radius $r_{\rm acc}$ is around 1 $R_\odot$. Therefore, the changes in the wind velocity profiles caused by X-ray ionization seen in Figure 8, will potentially have a very serious effect on the mass-accretion rate of the neutron star.

It is important to note that Figure 8 shows that major alterations in the wind dynamics result from relatively low X-ray luminosities. In actual MXRBs such as Vela X-1, the typical X-ray luminosities are at least 10^{36} ergs s^{-1}, i.e., at least one order of magnitude greater, and it is somewhat surprising that the wind can be affected so much by this low level of X-ray emission. However, as discussed in § IV*a*, the omission of optical depth effects can lead to a large underestimate of the force multiplier, and the quicker onset of X-ray dynamical alterations. If optical depth effects were included, the likely outcome would be that the dynamics would be qualitatively similar, but that the X-ray luminosity required to produce the same extent of change would have to be considerably larger.

TABLE 2

RESULTS FOR X-RAY ILLUMINATED STELLAR WIND MODELS

L_x (ergs s^{-1})	r_c (R_*)	$\log_{10} \xi_c$ (ergs cm s^{-1})	$d\dot{M}/d\Omega$ ($10^{-6}\ M_\odot$ yr^{-1} sr^{-1})	$v(r = 1.5\ R_*)$ (km s^{-1})
0	1.052	...	1.129	449.8
10^{33}	1.053	−3.60	1.113	436.4
10^{34}	1.053	−2.58	1.117	351.4
5×10^{34}	1.086	−1.67	1.004	211.1

c) *Applicability to Other Systems*

In addition to the MXRB systems and the related Be/X-ray binary systems (Van den Heuvel and Rappaport 1986), another likely application of this type of calculation concerns the line driven winds from accretion disks. Vitello and Shlosman (1988) have investigated the characteristics of radiatively driven models for winds from an accretion disk, finding that there are significant differences in the wind solutions for accretion disk systems compared to spherical systems, largely as a result from the differing geometry. Vitello and Shlosman (1988) found that the dynamics in the case of an accretion disk are more sensitive to ionization effects than a spherically symmetric model, and in particular that the existence of a steady line-driven wind from an accretion disk requires that ionization effects modify the wind dynamics in the vicinity of the critical point. Thus, calculations of the type presented here, in conjunction with realistic ionization and thermal structure calculations for the appropriate geometry and system parameters, are likely to prove essential to our understanding of winds from such objects as cataclysmic variables and active galactic nuclei.

Also, as mentioned above, these calculations are also likely to have application in the simulations of the dynamics in the winds of early-type star. Abbott and Friend (1989) have attempted very simple calculations concerning the effect of X-rays on the wind srructure of single stars, finding that the X-rays will tend to inhibit radiative driving, particularly in the outer, less dense regions of the wind, resulting in a reduced terminal velocity v_∞ compared to the case of unaffected wind dynamics. In OCR, the exponentially truncated power-law expression for the force multiplier (eq. [15]) was introduced in an *ad hoc* manner to limit the steepness of the rare factions found in the wind solutions, and thus, qualitatively, the effect of the X-rays could be, in an analogous manner, to limit the steepness of the shocks. Further discussion of this will be deferred to a future paper.

V. SUMMARY

The results presented in this paper can be summarized as follows. Calculations of the effect of changing ionization conditions on the radiative force multiplier $M(t)$ in an X-ray illuminated stellar wind, such as in a massive X-ray binary system like Vela X-1, have been presented. These calculations comprise a significant improvement over earlier calculations by MacGregor and Vitello (1982), who only included a very small number of lines in their calculations, whereas the results here show that a much larger number of lines contribute to the overall radiative force.

The variation of $M(t)$ with the ionization parameter ξ was found to be different than that assumed by Blondin *et al.* (1990) and Ho and Arons (1987), with the decline in $M(t)$ being considerably more gradual and complicated than assumed in those papers. Also estimates have been made of the effect of low-energy cutoffs in the X-ray spectrum and optical depth effects on the force multiplier results.

Some preliminary calculations of the structure of an X-ray illuminated stellar wind in an MXRB system have demonstrated that X-ray ionization will have a significant impact on

the wind dynamics, reducing the wind velocity by a large factor in certain regimes of the flow in MXRB systems. This in turn has major implications for the general behavior of MXRB systems.

Future work will involve constructing two-dimensional self consistent models of MXRBs using these results and extending them to include optical depth effects. It is also hoped to combine the force multiplier calculations presented here with the model of Blondin *et al.* (1990), and some early results from this study have already been presented (Blondin, Kallman, and Stevens 1990).

The authors thank D. Abbott for the use of the line list used in these calculations, and J. Blondin and S. Owocki for useful discussions through the course of this work.

REFERENCES

Abbott, D. C. 1980, *Ap. J.*, **242**, 1183.
———. 1982, *Ap. J.*, **259**, 282.
Abbott, M. J., and Friend, D. C. 1989, *Ap. J.*, **345**, 505.
Blondin, J. M., Kallman, T. R., Fryxell, B. A., and Taam, R. E. 1990, *Ap. J.*, **356**, 591.
Blondin, J. M., Kallman, T. R., and Stevens, I. R. 1990, *Bull. A.A.S.*, **21**, 1206.
Cameron, A. G. W. 1973, in *Explosive Nucleosynthesis*, ed. D. Schramm and W. D. Arnett (Austin: University of Texas Press), p. 3.
Castor, J. I. 1974, *M.N.R.A.S.*, **169**, 279.
Castor, J. I., Abbott, D. C., and Klein, R. I. 1975, *Ap. J.*, **195**, 157 (CAK).
Friend, D. B., and Castor, J. I. 1982, *Ap. J.*, **261**, 293.
Ho, C., and Arons, J. 1987, *Ap. J.*, **316**, 283.
Kallman, T. R., and McCray, R. 1982, *Ap. J. Suppl.*, **50**, 263.
Kallman, T. R., and White, N. E. 1982, *Ap. J. (Letters)*, **261**, L35.
Klein, R. I., and Castor, J. I. 1978, *Ap. J.*, **220**, 902.
Krolik, J., and Raymond, J. C. 1985, *Ap. J.*, **298**, 660.
MacGregor, K. B., and Vitello, P. A., **259**, 267 (MV).
Masai, K. 1984, *A. Space Sci.*, **106**, 391.
McCray, R., Kallman, T. R., Castor, J. I., and Olson, G. L. 1984, *Ap. J.*, **282**, 245.
Owocki, S. P., Castor, J. I., and Rybicki, G. B. 1988, *Ap. J.*, **335**, 914 (OCR).
Pauldrach, A., Puls, J., and Kudritzki, R. P. 1986, *Astr. Ap.*, **164**, 86.
Puls, J. 1987, *Astr. Ap.*, **184**, 227.
Reader, J., Corliss, C. H., Wiese, W. L., and Martin, G. A. 1980, *Wavelengths and Transition Probabilities for Atoms and Atomic Ions*, (NSRDS-NBS 68).
Smith, M. W., and Wiese, W. L. 1971, *Ap. J. Suppl.*, **23**, 103.
Stevens, I. R. 1988, *M.N.R.A.S.*, **232**, 199.
Tarter, C. B., Tucker, W. H., and Salpeter, E. E. 1969, *Ap. J.*, **233**, 334.
Van den Heuvel, E. P. J., and Rappaport, S. 1986, in *IAU Colloquium No. 92, Physics of Be Stars*, ed. A. Slettebak and T. D. Snow (Cambridge University Press), p. 291.
Vitello, P. A., and Shlosman, I. 1988, *Ap. J.*, **327**, 680.
White, N. E., Swank, J. H., and Holt, S. S. 1983, *Ap. J.*, **270**, 711.

TIMOTHY R. KALLMAN and IAN R. STEVENS: Code 665, NASA/Goddard Space Flight Center, Greenbelt, MD 20771